INTERNATIONAL JOURNAL FOR NUMERICAL METHODS IN FLUIDS
Int. J. Numer. Meth. Fluids 2000; **32**: 619–646

Analysis of iterative methods for the viscous/inviscid coupled problem via a spectral element approximation

Chuanju Xu* and Yumin Lin

Department of Mathematics, Xiamen University, Xiamen 361005, People's Republic of China

SUMMARY

Based on a new global variational formulation, a spectral element approximation of the incompressible Navier–Stokes/Euler coupled problem gives rise to a global discrete saddle problem. The classical Uzawa algorithm decouples the original saddle problem into two positive definite symmetric systems. Iterative solutions of such systems are feasible and attractive for large problems. It is shown that, provided an appropriate pre-conditioner is chosen for the pressure system, the nested conjugate gradient methods can be applied to obtain rapid convergence rates. Detailed numerical examples are given to prove the quality of the pre-conditioner. Thanks to the rapid iterative convergence, the global Uzawa algorithm takes advantage of this as compared with the classical iteration by sub-domain procedures. Furthermore, a generalization of the pre-conditioned iterative algorithm to flow simulation is carried out. Comparisons of computational complexity between the Navier–Stokes/Euler coupled solution and the full Navier–Stokes solution are made. It is shown that the gain obtained by using the Navier–Stokes/Euler coupled solution is generally considerable. Copyright © 2000 John Wiley & Sons, Ltd.

KEY WORDS: global Uzawa algorithm; Navier–Stokes/Euler coupled equations; pre-conditioned conjugate gradient method; spectral element approximation

1. INTRODUCTION

Domain decomposition methods are useful approximation techniques to deal with computational fluid dynamics (CFD) problems, especially in complex physical domains and when using parallel computational environments. They were first employed in finite difference and finite element methods. In the context of spectral methods, they date from the late 1970s (see for instance Reference [1] and the references therein). Earlier applications of the domain decomposition methods are related to splitting the whole domain into sub-domains of simpler shape, and then reducing the given problem to a sequence of sub-problems, which include generally the same equations. Recently, a lot of attention has been focused on the possibility of using different types of equations within sub-domains where different flow characters are observable.

* Correspondence to: Department of Mathematics, Xiamen University, 361005 Xiamen, People's Republic of China.

Received 15 May 1998
Revised 18 April 1999

There has been some work on the coupling of compressible viscous and inviscid equations [2–4]. The coupled problem of incompressible viscous and inviscid equations has been considered by Dinh *et al*. [5] and Xu *et al*. [6–8]. One of main goals of these investigations had been to find the correct conditions on the interface separating the viscous and inviscid sub-domain. However, efficient solvers are also of great importance when solving numerically the full time-dependent coupled equations. Before the work of Xu and Maday [8], numerical algorithms used to solve the resulting discrete coupled equations were always 'iteration by sub-domain resolution'—known as the alternating Schwarz method [3,9,32]. An effective iteration by sub-domain procedure, however, requires exact convergence analysis and a certain number of repeat resolutions to reach convergence, which is often theoretically non-trivial and numerically costly.

In Reference [8], a new coupling strategy for the incompressible viscous/inviscid coupled equations was introduced. This strategy consists of writing the viscous/inviscid coupled equations into a global variational formulation. Thanks to this new weak formulation, the original coupled equations are written under a global saddle problem, similar to the one resulting from the full Stokes equations. Therefore, standard techniques developed for the Stokes problem can be applied (after some modifications) to solve the viscous/inviscid coupled equations.

To understand what approaches can be used to solve discrete systems based on the global saddle problem of the Navier–Stokes/Euler coupled equations, numerous approaches that have been proposed for solving the algebraic system stemming from discretization of the Stokes equations are recalled. One approach is to solve the nodal pressure and velocity unknowns directly in coupled form [10,11]. A second approach is to replace the continuity equations with a Poisson equation for the pressure [12–15]. A third approach is to apply block Gaussian elimination and back-substitution for the pressure and the velocity yielding two positive definite symmetric systems (see, for example, Reference [16] and the references therein). The first approach is general and robust; however, it can be memory intensive for large problems, in particular those with high-order approximation. The second approach decouples the momentum and continuity except on the domain boundary; however, it may require a rediscretization of the continuous problem, and boundary conditions must be supplied for the pressure.

The third approach mentioned above is chosen, in this paper, to solve the discrete system resulting from the discretization of the unsteady Navier–Stokes/Euler coupled equations for the following reasons: first, between numerous algorithms, the Uzawa decoupling procedure has been proven to be more attractive in terms of computational complexity and memory requirement than a direct algorithm [16]; second, the block diagonal structure in the velocity system allows us to inverse the velocity matrix easily, and therefore reduce the cost in each iteration for the pressure calculation; third, the Uzawa decoupling procedure has been successfully applied to the pure Navier–Stokes solution, choosing the same algorithm to solve the discrete Navier–Stockes/Euler coupled equations enables us to compare the CPU costs with the pure Navier–Stokes solution in an easier way.

In Reference [8] a conjugate gradient iterative algorithm has been applied to solve both the pressure algebraic system and the velocity algebraic system. However, numerical experiments showed that the direct gradient algorithm applied to the pressure algebraic system converges

slowly and too many iterations are required to obtain sufficient accuracy. The present work follows the subject of Reference [8], and considers furthermore a preconditioning method to accelerate the rate of convergence. We give detailed analysis of the preconditioned Uzawa algorithm, with special emphasis on solving the algebraic equations resulting from spectral element approximation of the Navier–Stokes/Euler coupled equations. Numerical results show that appropriate pre-conditioner applied to the pressure system can significantly recover the rapid convergence rate, as done by similar pre-conditioiners applied to a pure Navier–Stokes pressure system.

The outline of this paper is as follow: in Section 2 the basic Navier–Stokes/Euler coupled equations and the global variational formulation are recalled. Section 3 proposes a spectral element approximation based on the global variational formulation. Section 4 reviews the Uzawa method for the unsteady Stokes problem, and then shows how the Uzawa algorithm can be extended to the unsteady viscous/inviscid coupled problem. In Section 5, numerical tests and comparisons with the full Stokes solution show the quality of the pre-conditioner proposed. In Section 6, the viscous/inviscid coupled problem is extended to the unsteady Navier–Stokes/Euler coupled problem. Flow simulations are carried out to prove the gain of the new coupling strategy. The computational complexity will be discussed in Section 7. Finally, Section 8 concludes the paper.

1.1. Notation

We assume Ω be a bounded, connected, open subset of $\mathbb{R}^d$ ($d = 2$ or 3), with boundary $\partial\Omega$; Ω^- and Ω^+ are two open sub-sets of Ω, with $\Omega^- \cap \Omega^+ = \varnothing$, $\bar{\Omega}^- \cup \bar{\Omega}^+ = \bar{\Omega}$. $\Gamma^k = \partial\Omega \cap \partial\Omega^k$, $k = -, +$; $\Gamma = \partial\Omega^- \cap \partial\Omega^+$.

In the following, we use letters of boldface type to denote vectors and vector functions. All the quantities defined in Ω^k ($k = -, +$) are identified by a superscript k. For example, if φ is a function defined in Ω then the restriction of φ in Ω^k is denoted by φ^k. Let $\mathbf{n}$ be the outward unit normal on $\partial\Omega$ to Ω, and $\mathbf{n}^-$, $\mathbf{n}^+$ be the outward unit normals on Γ to Ω^-, Ω^+ respectively (see Figure 1). For all $m \geq 0$, we denote by $H^m(\Omega)$ the classical Sobolev spaces, provided with the usual norm $\|\cdot\|_{m,\Omega}$, and also with the semi-norm $|\cdot|_{m,\Omega}$. We consider also the space $L^\infty(\Omega)$ with the norm $\|\cdot\|_{L^\infty\Omega}$. For any integer N, we denote $\mathbb{P}_N(\Omega)$ to be the set of all polynomials of degree $\leq N$ in Ω. $c_0, c, c_1, \ldots$ are generic positive constants independent of

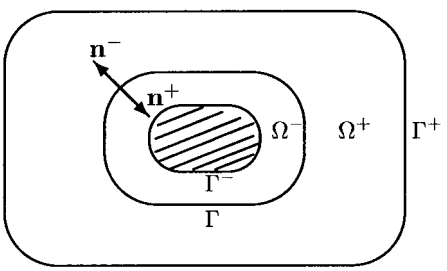

Figure 1. Model of two-dimensional domain.

discretization parameters N and Δt, but dependent possibly on the exact solutions of the equations under considerations. We will need the space $L_0^2(\Omega)$, the space of all functions, which are square integrable over Ω with zero average.

2. VISCOUS/INVISCID COUPLED PROBLEM

We consider the following viscous/inviscid coupled problem: for $\mathbf{f}$ given in $L^2(\Omega)^d$, find a velocity $\mathbf{u}$ and a pressure p, such that

$$\begin{cases} \alpha\mathbf{u}^- - \nu\Delta\mathbf{u}^- + \nabla p^- = \mathbf{f}^+, & \nabla\cdot\mathbf{u}^- = 0 \quad \text{in } \Omega^- \\ \alpha\mathbf{u}^+ + \nabla p^+ = \mathbf{f}^+, & \nabla\cdot\mathbf{u}^+ = 0 \quad \text{in } \Omega^- \\ \mathbf{u}^- = 0 & \text{on } \Gamma^- \\ \mathbf{u}^+\cdot\mathbf{n} = 0 & \text{on } \Gamma^- \end{cases} \tag{1}$$

where α and ν are positive constants. The coupled problem (1) is of interest not only in its own right, but also in that it constitutes the principal part in solving the full Navier–Stokes/Euler coupled equations. In this respect, α can be viewed as the inverse of the time step, ν is the viscosity, $\mathbf{f}$ is an augmented force, which includes the explicitly treated convective term.

Obviously, appropriate conditions on the interface Γ separating the two sub-domains Ω^-, Ω^+ are required. We have shown in our previous papers (see Reference [8]) that the solutions $(\mathbf{u}^-, p^-)$ on the viscous domain Ω^- and $(\mathbf{u}^+, p^+)$ on the inviscid domain Ω^+ are related through the equations

$$\begin{cases} \nu\dfrac{\partial\mathbf{u}^-}{\partial\mathbf{n}^-} - p^-\cdot\mathbf{n}^- = p^+\cdot\mathbf{n}^+ & \text{on } \Gamma \\ -\mathbf{u}^-\cdot\mathbf{n}^- = -\mathbf{u}^+\cdot\mathbf{n}^+ & \text{on } \Gamma \end{cases} \tag{2}$$

The well-posedness of the Equations (1) and (2) can be proven either by an *artificial viscosity method* or by a globally variational method. From the practical point of view, the latter is of particular interest. This fact will be demonstrated at the end of this paper. We review briefly the basic idea. The equivalent variational formulation of (1) and (2) is:
Find $(\mathbf{u}, p)$ in $X \times M$ such that for all $\mathbf{v}$ in X, all q in M,

$$\alpha(\mathbf{u}, \mathbf{v}) + \nu(\nabla\mathbf{u}^-, \nabla\mathbf{v}^-)^- - (p^-, \nabla\cdot\mathbf{v}^-)^- + (\nabla p^+, \mathbf{v}^+)^+ - (p^+\cdot\mathbf{n}^+, \mathbf{v}^-)^\Gamma = (\mathbf{f}, \mathbf{v}),$$

$$(\nabla\cdot\mathbf{u}^-, q^-)^- - (\mathbf{u}^+, \nabla q^+)^+ - (\mathbf{u}^-\cdot\mathbf{n}^+, q^+)^\Gamma = 0 \tag{3}$$

where $(\cdot,\cdot)^k$, $k = -, +$, $(\cdot,\cdot)^\Gamma$, are defined respectively by

$$(\Phi, \Psi)^k = \int_{\Omega^k} \Phi\Psi, \qquad (\Phi, \Psi) = (\Phi, \Psi)^- + (\Phi, \Psi)^+, \qquad (\Phi, \Psi)^\Gamma = \int_\Gamma \Phi\Psi$$

The spaces for $\mathbf{u}$ and p such that (3) be well posed are

$$X = \{\mathbf{v}|_{\Omega^-} \in H^1(\Omega^-)^d,\ \mathbf{v}|_{\Omega^+} \in L^2(\Omega^+)^d,\ \mathbf{v}|_{\Gamma^-} = 0\}$$

$$M = \{q|_{\Omega^-} \in L^2(\Omega^-),\ q|_{\Omega^+} \in H^1(\Omega^+)\} \cap L_0^2(\Omega) \tag{4}$$

provided with the norms

$$\|\mathbf{v}\|_X = \|\mathbf{v}^-\|_{1,\Omega^-} + \|\mathbf{v}^+\|_{0,\Omega^+}, \qquad \|q\|_M = \|q^-\|_{0,\Omega^-} + \|q^+\|_{1,\Omega^+}$$

The equivalence between Equations (1)–(2) and (3) can be seen as follow. From Equations (1) and (2), Equation (3) can be deduced readily; reciprocally, for all $\mathbf{v}^- \in H^1(\Omega^-)^d$, $\mathbf{v}^-|_{\Gamma^-} = 0$ and all $q^- \in L_0^2(\Omega^-)$, let in Equation (3)

$$\mathbf{v} = \begin{cases} \mathbf{v}^- & \Omega^- \\ 0 & \Omega^+ \end{cases}, \qquad q = \begin{cases} q^- & \Omega^- \\ 0 & \Omega^+ \end{cases}$$

we have

$$\alpha(\mathbf{u}^-, \mathbf{v}^-)^- + \nu(\nabla\mathbf{u}^-, \nabla\mathbf{v}^-)^- - (p^-, \nabla\cdot\mathbf{v}^-)^- = (p^+\cdot\mathbf{n}^+, \mathbf{v}^-)^\Gamma + (\mathbf{f}^-, \mathbf{v}^-)^-,$$

$$(\nabla\cdot\mathbf{u}^-, q^-)^- = 0$$

which give the viscous equations and the first of interface conditions (2) in the sense of $H^{-1/2}(\Gamma)$.

In another part, for all $\mathbf{v}^+ \in L^2(\Omega^+)^d$, and all $q^+ \in H^1(\Omega^+) \cap L_0^2(\Omega^+)$, let in Equation (3)

$$\mathbf{v} = \begin{cases} 0 & \Omega^- \\ \mathbf{v}^+ & \Omega^+ \end{cases}, \qquad q = \begin{cases} 0 & \Omega^- \\ q^+ & \Omega^+ \end{cases}$$

then we obtain

$$\alpha(\mathbf{u}^+, \mathbf{v}^+)^+ + (\nabla p^+, \mathbf{v}^+)^+ = (\mathbf{f}^+, \mathbf{v}^+)^+$$

$$-(\mathbf{u}^+, \nabla q^+)^+ = (\mathbf{u}^-\cdot\mathbf{n}^-, q^+)^\Gamma$$

which give the inviscid equations and the second of interface conditions (2) in the sense of $H^{-1/2}(\Gamma)$.

To prove the well-posedness of the variational problem (3), we write Equation (3) into the following equivalent saddle-point problem:
Find $(\mathbf{u}, p)$ in $(X \times M)$ such that

$$\begin{cases} a(\mathbf{u}, \mathbf{v}) + b(\mathbf{v}, p) = (\mathbf{f}, \mathbf{v}) & \forall \mathbf{v} \in X \\ b(\mathbf{u}, q) = 0 & \forall q \in M \end{cases} \tag{5}$$

where the bilinear form a and b are defined by

$$a(\mathbf{u}, \mathbf{v}) = \alpha(\mathbf{u}, \mathbf{v}) + \nu(\nabla \mathbf{u}, \nabla \mathbf{v})^- \quad \forall \mathbf{u}, \mathbf{v} \in X$$

$$b(\mathbf{v}, q) = -(q, \nabla \cdot \mathbf{v})^- + (\nabla q, \mathbf{v})^+ - (q^+ \cdot \mathbf{n}^+, \mathbf{v}^-)^\Gamma \quad \forall \mathbf{v} \in X,\ q \in M$$

Note that the form a is continuous and coercive in $X \times X$, while the form b is continuous and satisfies the Babuska–Brezzi's *Inf–Sup* condition in $X \times M$ (see Reference [8] for the detailed proof). The well-posedness of problem (5) can be proven by applying the standard saddle-point theory (see e.g. References [17,18]).

3. SPECTRAL DISCRETIZATION

A classical method of solving coupled problems consists of exhibiting its solution as a limit of solutions of two sub-problems within Ω^- and Ω^+. This is achieved by considering the following iterative procedure:
First, one of the two sub-problems, in Ω^- for instance,

$$\begin{cases} \alpha \mathbf{u} - \nu \Delta \mathbf{u} + \nabla p = \mathbf{f}, \quad \nabla \cdot \mathbf{u} = 0 & \text{in } \Omega^- \\ \mathbf{u} = 0 & \text{on } \Gamma^- \\ \nu \dfrac{\partial \mathbf{u}}{\partial \mathbf{n}^-} - p^+ \cdot \mathbf{n}^- = p^+ \cdot \mathbf{n}^+ & \text{on } \Gamma \end{cases}$$

is solved with a Neumann condition $p^+ \cdot \mathbf{n}^+$ arbitrarily; then knowing $\mathbf{u}^-$ on Γ, we solve the other sub-problem,

$$\begin{cases} \alpha \mathbf{u} + \nabla p = \mathbf{f}, \quad \nabla \cdot \mathbf{u} = 0 & \text{in } \Omega^+ \\ \mathbf{u} \cdot \mathbf{n}^+ = 0 & \text{on } \Gamma^+ \\ \mathbf{u} \cdot \mathbf{n}^+ = \mathbf{u}^- \cdot \mathbf{n}^+ & \text{on } \Gamma \end{cases}$$

which gives p^+; and so on. The iterative procedure continues until the convergence is reached. The effectiveness of this strategy depends on the existence of convergence results of the iterative procedure (generally a relaxation parameter is needed to accelerate the convergence). It requires a certain number of repeat resolutions to reach convergence, which could be expensive if the convergence rate is slow. We relegate these subjects to other papers (see Reference [19]).

However, we choose the strategy called 'global resolution'. We are going to see that this strategy is very attractive in terms of computational complexity thanks to an effective pre-conditioned conjugate gradient iteration based on an Uzawa decoupled procedure.

We begin by introducing some basic notations. For a matter of simplification, consider a rectangular domain Ω, which is split into two rectangular sub-domains Ω^- and Ω^+. Let $(\cdot,\cdot)_{\mathrm{GL}}$, $(\cdot,\cdot)_{\mathrm{G}}$ to be evaluations of the continuous inner product $(\cdot,\cdot)$ by Gauss–Lobatto (GL) and Gauss (G) quadrature respectively. The following well-known identity and inequality [20] will be used:

$$(\varphi, 1)^k_{\mathrm{G}} = (\varphi, 1)^k_{\mathrm{GL}} = \int_{\Omega^k} \varphi \, \mathrm{d}\mathbf{x}, \quad \forall \varphi \in \mathbb{P}_{2N-1}(\Omega^k), \quad k = -, + \tag{6}$$

$$\int_{\Omega^k} \varphi^2 \, \mathrm{d}\mathbf{x} \le (\varphi, \varphi)^k_{\mathrm{GL}} \le c \int_{\Omega^k} \varphi^2 \, \mathrm{d}\mathbf{x}, \quad \forall \varphi \in \mathbb{P}_N(\Omega^k), \quad k = -, + \tag{7}$$

We introduce two discrete spaces

$$X_N = X \cap (\mathbb{P}_N(\Omega^-) \times \mathbb{P}_N(\Omega^+)), \qquad M_N = M \cap (\mathbb{P}_{N-2}(\Omega^-) \times \mathbb{P}_N(\Omega^+))$$

endowed with the norms of X and M respectively.

We now consider a spectral approximation to the viscous/inviscid coupled problem based on the variational form (3):
Find $(\mathbf{u}_N, p_N) \in X_N \times M_N$ such that

$$\begin{cases} a_N(\mathbf{u}_N, \mathbf{v}_N) + b_N(\mathbf{v}_N, p_N) = (\mathbf{f}, \mathbf{v}_N)_{\mathrm{GL}} & \forall \mathbf{v}_N \in X_N \\ b_N(\mathbf{u}_N, q_N) = 0 & \forall q_N \in M_N \end{cases} \tag{8}$$

where a_N and b_N are two bilinear forms, defined by

$$a_N(\mathbf{u}_N, \mathbf{v}_N) = \alpha(\mathbf{u}_N, \mathbf{v}_N)_{\mathrm{GL}} + \nu(\nabla \mathbf{u}_N^-, \nabla \mathbf{v}_N^-)^-_{\mathrm{GL}}, \quad \forall \mathbf{u}_N, \mathbf{v}_N \in X_N$$

$$b_N(\mathbf{v}_N, q_N) = -(q_N^-, \nabla \cdot \mathbf{v}_N^-)^-_{\mathrm{G}} + (\nabla q_N^+, \mathbf{v}_N^+)^+_{\mathrm{GL}} + (q_N^+, \mathbf{v}_N^- \cdot \mathbf{n}^-)^\Gamma_{\mathrm{GL}}, \quad \forall \mathbf{v}_N \in X_N, \ q_N \in M_N$$

Theorem 3.1
The discrete problem (8) is well posed.

Proof
The theorem is proved by applying the standard saddle-point theorem. It consists on verifying the following properties:

- The coercivity and the continuity of the mapping $(\mathbf{u}_N, \mathbf{v}_N) \mapsto a_N(\mathbf{u}_N, \mathbf{v}_N)$ in $X_N \times X_N$, which are trivial according to the inequality (7).
- The form b_N is continuous. In fact, for all $\mathbf{v}_N \in X_N$, $q_N \in M_N$,

$$\begin{aligned} b_N(\mathbf{v}_N, q_N) &\le \|q_N^-\|_{0,\Omega^-} |\mathbf{v}_N^-|_{1,\Omega^-} + c|q_N^+|_{1,\Omega^+} \|\mathbf{v}_N^+\|_{0,\Omega^+} + c\|q_N^+\|_{0,\Gamma} \|\mathbf{v}_N^- \cdot \mathbf{n}^-\|_{0,\Gamma} \\ &\le \gamma \|q_N\|_M \|\mathbf{v}_N^-\|_X \end{aligned}$$

where γ is a constant depending on the continuous trace mapping constant from $H^1(\Omega^-)$ or $H^1(\Omega^+)$ to $H^{1/2}(\Gamma)$.

- The *Inf–Sup* condition of b_N in $X_N \times M_N$, which is demonstrated in the following lemma. □

Lemma 3.1
Assume β_N^- be a positive constant such that

$$\inf_{q_N^- \in L_0^2(\Omega^-) \cap \mathbb{P}_{N-2}(\Omega^-)} \sup_{\mathbf{v}_N^- \in H_0^1(\Omega^-)^d \cap \mathbb{P}_N(\Omega^-)^d} \frac{-(q_N^-, \nabla \cdot \mathbf{v}_N^-)_G^-}{\|\mathbf{v}_N^-\|_{1,\Omega^-} \|q_N^-\|_{0,\Omega^-}} \geq \beta_N^-$$

then there exists a constant $\beta_N = c\beta_N^-/(1+\beta_N^-)$, such that

$$\inf_{q_N \in M_N} \sup_{\mathbf{v}_N \in X_N} \frac{b_N(\mathbf{v}_N, q_N)}{\|\mathbf{v}_N\|_X \|q_N\|_M} \geq \beta_N \tag{9}$$

Proof
Let $q \in M_N$, we have $q^- \in \mathbb{P}_{N-2}(\Omega^-)$. Decompose q^- by

$$q^- = q_0^- + \tilde{q}^- \tag{10}$$

such that $q_0^- \in L_0^2(\Omega^-) \cap \mathbb{P}_{N-2}(\Omega^-)$ and $\tilde{q}^-$ is constant in Ω^-. It is known that for such q_0^-, there exists a function $\mathbf{v}_0^- \in H_0^1(\Omega^-)^d \cap \mathbb{P}_N(\Omega^-)^d$ such that

$$\nabla \cdot \mathbf{v}_0^- = -q_0^- \quad \text{and} \quad \|\mathbf{v}_0^-\|_{1,\Omega^-} \leq \frac{1}{\beta_N^-} \|q_0^-\|_{0,\Omega^-} \tag{11}$$

We fix a function $\mathbf{v}' \in X_N$ which satisfies $\int_\Gamma \mathbf{v}' \cdot \mathbf{n}^- = 1$ and let $\mathbf{w}_0$ be a function of $H_0^1(\Omega^-)^d \cap \mathbb{P}_N(\Omega^-)^d$, such that

$$\int_{\Omega^-} (\nabla \cdot \mathbf{w}_0) q = \int_{\Omega^-} (\nabla \cdot \mathbf{v}') q, \quad \forall q \in L_0^2(\Omega^-) \cap \mathbb{P}_{N-2}(\Omega^-) \tag{12}$$

If we define $\tilde{\mathbf{v}}^- = \mathbf{v}' - \mathbf{w}_0$, then the function $\tilde{\mathbf{v}}^-$ satisfies

$$\int_{\Omega^-} (\nabla \cdot \tilde{\mathbf{v}}^-) q = 0, \quad \forall q \in L_0^2(\Omega^-) \cap \mathbb{P}_{N-2}(\Omega^-), \qquad \int_\Gamma \tilde{\mathbf{v}}^- \cdot \mathbf{n}^- = 1 \tag{13}$$

Taking $\mathbf{v}^- = \mathbf{v}_0^- - \tilde{q}^- \tilde{\mathbf{v}}^-$, we obtain by using Equations (10), (11) and (13)

$$-(q^-, \nabla \cdot \mathbf{v}^-)_G^- = -\int_{\Omega^-} (q_0^- + \tilde{q}^-) \nabla \cdot (\mathbf{v}_0^- - \tilde{q}^- \tilde{\mathbf{v}}^-) = \|q_0^-\|_{0,\Omega^-}^2 + (\tilde{q}^-)^2 \tag{14}$$

In the sub-domain Ω^+, the same decomposition as (10) gives

$$q^+ = q_0^+ + \tilde{q}^+ \tag{15}$$

with $q_0^+ \in L_0^2(\Omega^+) \cap \mathbb{P}_N(\Omega^+)$ and $\tilde{q}^+$ is constant in Ω^+. Let $\mathbf{v}_0^+ = \nabla q_0^+$, then

$$(\nabla q_0^+, \mathbf{v}_0^+)_{\mathrm{GL}}^+ \geq \|\nabla q_0^+\|_{0,\Omega^+}^2 = |q_0^+|_{1,\Omega^+} \|\mathbf{v}_0^+\|_{0,\Omega^+} \tag{16}$$

Let $\mathbf{z} \in L_0^2(\Omega^+)^d \cap \mathbb{P}_N(\Omega^+)^d$ such that

$$(\mathbf{z}, \nabla q)_{\mathrm{GL}}^+ = (q, \tilde{\mathbf{v}}^- \cdot \mathbf{n}^-)_{\mathrm{GL}}^\Gamma \quad \forall q L_0^2(\Omega^+) \cap \mathbb{P}_N(\Omega^+) \tag{17}$$

Taking $\mathbf{v}^+ = \mathbf{v}_0^+ + \tilde{q}^- \mathbf{z}$ and noting that $\tilde{q}^- |\Omega^-| + \tilde{q}^+ |\Omega^+| = 0$, then

$$\begin{aligned}
&(\nabla q^+, \mathbf{v}^+)_{\mathrm{GL}}^+ + (q^+, \mathbf{v}^- \cdot \mathbf{n}^-)_{\mathrm{GL}}^\Gamma \\
&= (\nabla q^+, \mathbf{v}_0^+)_{\mathrm{GL}}^+ + (\nabla q^+, \tilde{q}^- \mathbf{z})_{\mathrm{GL}}^+ + (q_0^+, \mathbf{v}^- \cdot \mathbf{n}^-)_{\mathrm{GL}}^\Gamma + (\tilde{q}^+, \mathbf{v}^- \cdot \mathbf{n}^-)_{\mathrm{GL}}^\Gamma \\
&\geq |q^+|_{1,\Omega^+}^2 + (q_0^+, \mathbf{v}_0^- \cdot \mathbf{n}^-)_{\mathrm{GL}}^\Gamma + \tilde{q}^+ (1, \mathbf{v}^- \cdot \mathbf{n}^-)_{\mathrm{GL}}^\Gamma = |q^+|_{1,\Omega^+}^2 - \tilde{q}^- \tilde{q}^+ \\
&= |q^+|_{1,\Omega}^2 + |\Omega^+|/|\Omega^-|(\tilde{q}^+)^2
\end{aligned} \tag{18}$$

where $|\Omega^k|$ is the measure of Ω^k. To estimate $\mathbf{v}^-$ and $\mathbf{v}^+$, we use Equations (11), (12), (17) and the definition of $\tilde{\mathbf{v}}^-$,

$$\|\mathbf{v}^-\|_{1,\Omega^-} = \|\mathbf{v}_0^- - \tilde{q}^- \tilde{\mathbf{v}}^-\|_{1,\Omega^-} \leq \frac{1}{\beta_N^-} \|q_0^-\|_{0,\Omega^-} + c\tilde{q}^- \leq \frac{c_1}{\beta_N^-} \|q^-\|_{0,\Omega^-} \tag{19}$$

$$\|\mathbf{v}^+\|_{0,\Omega^+} \leq \|\mathbf{v}_0^+\|_{0,\Omega^+} + \tilde{q}^- \|\tilde{\mathbf{v}}^-\|_{1,\Omega^-} \leq |q_0^+|_{1,\Omega^+} + c_2 \tilde{q}^+ \leq c_3 \|q^+\|_{1,\Omega^+} \tag{20}$$

where c, c_1, c_2 and c_3 depend on $\mathbf{v}'$, Ω^- and Ω^+. Taking $\mathbf{v} = (\mathbf{v}^-, \mathbf{v}^+)$, we then have $\mathbf{v} \in X$; furthermore using Equations (14), (18)–(20), we get

$$\begin{aligned}
\frac{b_N(\mathbf{v}, q)}{\|\mathbf{v}\|_X} &= \frac{-(q^-, \nabla \cdot \mathbf{v}^-)_{\mathrm{G}}^- + (\nabla q^+, \mathbf{v}^+)_{\mathrm{GL}}^+ + (q^+, \mathbf{v}^- \cdot \mathbf{n}^-)_{\mathrm{GL}}^\Gamma}{\|\mathbf{v}^-\|_{1,\Omega^-} + \|\mathbf{v}^+\|_{0,\Omega^+}} \\
&\geq \frac{\|q_0^-\|_{0,\Omega^-}^2 + (\tilde{q}^-)^2 + |q^+|_{1,\Omega^+}^2 + |\Omega^+|/|\Omega^-|(\tilde{q}^+)^2}{(c_1/\beta_N^-)\|q^-\|_{0,\Omega^-} + c_3 \|q^+\|_{1,\Omega^+}} \geq \beta_N \|q\|_M
\end{aligned}$$

with $\beta_N = c\beta_N^-/(1 + \beta_N^-)$, where c is a constant depending on the domain. □

Remark 3.1

It has been theoretically proven that the local *Inf–Sup* constant β_N^- satisfies $\beta_N^- \simeq cN^{-1/2}$, while numerical evidences show [21] a comportment as $O(N^{-1/4})$. Lemma 3.1 implicates that $\beta_N \simeq \beta_N^-$, i.e. the global *Inf–Sup* constant has a comportment similar to the local *Inf–Sup*

constant. This fact will guarantee the effectiveness of the numerical algorithm described below.

4. THE UZAWA ALGORITHM

Hereafter, we use letters of boldface lower type to denote vectors or vector functions and use letters of boldface upper type to denote matrices. Expressing $\mathbf{u}_N$, $\mathbf{v}_N$, p_N and q_N in Lagrangian interpolants, and choosing each test function $\mathbf{v}_N$, q_N to be non-zero at only one global collocation point, we obtain from the problem (8) the following algebraic equations given in matrix form:

$$\begin{pmatrix} \mathbf{H}^- & 0 \\ 0 & \mathbf{H}^+ \end{pmatrix}\begin{pmatrix} \mathbf{u}^- \\ \mathbf{u}^+ \end{pmatrix} - \begin{pmatrix} \mathbf{D}^- & 0 \\ \mathbf{I}^\Gamma & -(\mathbf{D}^+)^{\mathrm{T}} \end{pmatrix}^T \begin{pmatrix} \mathbf{p}^- \\ \mathbf{p}^+ \end{pmatrix} = \begin{pmatrix} \mathbf{B}^- \mathbf{f}^- \\ \mathbf{B}^+ \mathbf{f}^+ \end{pmatrix} \tag{21}$$

$$-\begin{pmatrix} \mathbf{D}^- & 0 \\ \mathbf{I}^\Gamma & -(\mathbf{D}^+)^T \end{pmatrix}\begin{pmatrix} \mathbf{u}^- \\ \mathbf{u}^+ \end{pmatrix} = \begin{pmatrix} 0 \\ 0 \end{pmatrix} \tag{22}$$

It is assumed that the homogeneous boundary conditions on the viscous domain are imposed by eliminating appropriate row and columns. In (21) and (22), the unknowns $\mathbf{u}^k$, p^k ($k = -, +$) are the values at the global collocation points of the velocity and the pressure; $\mathbf{D}^-$ and $(\mathbf{D}^+)^T$ are the discrete divergence operators stemming from $(\nabla\cdot\mathbf{u}_N^-, q_N^-)_{\mathrm{G}}^-$ and $(\mathbf{u}_N^+, \nabla q_N^+)_{\mathrm{GL}}^+$ respectively; the superscript T denotes the transposition of matrix; $\mathbf{B}^-$ and $\mathbf{B}^+$ are the associated mass matrices; $\mathbf{I}^\Gamma$ denotes the identity operator applied in the normal $\mathbf{n}^-$ on the interface Γ (under implication of multiplication by the weights corresponding on Γ); $\mathbf{H}^k$ ($k = -, +$) is defined by

$$\mathbf{H}^k = \alpha\mathbf{B}^k + \nu\delta_{k^-}\mathbf{A}^-$$

where

$$\delta_{k^-} = \begin{cases} 1 & k = - \\ 0 & k = + \end{cases}$$

and $\mathbf{A}^-$ is the discrete Laplace operator.

To simplify the notations, let us denote

$$\mathbf{H}_c = \begin{pmatrix} \mathbf{H}^- & 0 \\ 0 & \mathbf{H}^+ \end{pmatrix}, \qquad \mathbf{D}_c = \begin{pmatrix} \mathbf{D}^- & 0 \\ \mathbf{I}^\Gamma & -(\mathbf{D}^+)^T \end{pmatrix}, \qquad \mathbf{B}_c = \begin{pmatrix} \mathbf{B}^- & 0 \\ 0 & \mathbf{B}^+ \end{pmatrix},$$

$$\mathbf{u}_c = \begin{pmatrix} \mathbf{u}^- \\ \mathbf{u}^+ \end{pmatrix}, \ldots$$

We can rewrite (21) and (22) into

$$\begin{cases} \mathbf{H}_c\mathbf{u}_c - \mathbf{D}_c^T\mathbf{p}_c = \mathrm{B}_c\mathbf{f}_c \\ -\mathbf{D}_c\mathbf{u}_c = 0 \end{cases} \tag{23}$$

We then break the saddle problem (23) into two positive definite symmetric forms, one for the global pressure and one for the global velocity,

$$\mathbf{S}_c\mathbf{p}_c = -\mathbf{D}_c\mathbf{H}_c^{-1}\mathbf{B}_c\mathbf{f}_c \tag{24}$$

$$\mathbf{H}_c\mathbf{u}_c = \mathbf{D}_c^T\mathbf{p}_c + \mathbf{B}_c\mathbf{f}_c \tag{25}$$

where

$$\mathbf{S}_c = \mathbf{D}_c\mathbf{H}_c^{-1}\mathbf{D}_c^T \tag{26}$$

The advantage of the Uzawa procedure is that the pressure and velocity are completely decoupled in the resolution. The apparent disadvantage is the system in the discrete pressure, as the matrix $\mathbf{S}_c$, has rank equal to the number of global pressure degrees of freedom, and is coupled at the interface due to the presence of $\mathbf{I}^\Gamma$, and thus necessitates an iterative solver. Note that $\mathbf{S}_c$ and $\mathbf{H}_c$ are positive definite symmetric matrices, standard elliptic solvers like conjugate gradient algorithm can readily be applied to solve the discrete pressure equation (24) and the discrete velocity equation (25). An important point to note is that the matrix $\mathbf{H}_c$ in $\mathbf{S}_c$ is diagonal by block at the interface level, which means that the inverse of $\mathbf{H}_c$ can be done separately between the viscous part and the inviscid part. We see that inverse of $\mathbf{H}^+$ is immediate, while $\mathbf{H}^-$ represents the standard Helmholtz operator and can be inverted by well pre-conditioned conjugate gradient iterations (see e.g. References [22,23]).

In summary, the pressure is calculated by an inner/outer pre-conditioned conjugate gradient iterative procedure. At each iteration, one inverse of $\mathbf{H}_c$ has to be done, which will be effected by an inner iterative procedure. In order for this inner/outer procedure to be efficient for large problems, a good pre-conditioner $\mathbf{P}_c$ needs to be found to accelerate the convergence of the outer conjugate gradient algorithm.

To find appropriate pre-conditioners to the matrix $\mathbf{S}_c$, we first review some fast spectral element solvers of currently used in the resolution of the unsteady Stokes problem: the first solver uses a two-level Richardson inner/outer iteration scheme [24]; the second solver uses the approach of Cahouet and Chabard [22], i.e. pre-condition the pressure matrix $\mathbf{S}_c$ directly. Numerical tests show that the second solver is simpler and more efficient (see e.g. Reference [16] and the references therein). Therefore, we are particularly interested in the second approach, which we briefly recall as follows. Suppose we deal with the semi-discretized unsteady Stokes problem in the *whole* domain Ω,

$$\alpha\mathbf{u} - \nu\Delta\mathbf{u} + \nabla p = \mathbf{f}, \qquad \nabla\cdot\mathbf{u} = 0 \quad \text{in } \Omega \tag{27}$$

subject to the homogeneous Dirichlet velocity boundary conditions on the whole domain boundary $\partial\Omega$. Consider its spectral approximation based on suitable variational form:
Find $\mathbf{u}_N \times p_N \in X'_N \times M'_N$, such that

$$\begin{cases} \alpha(\mathbf{u}_N, \mathbf{v}_N)_{\mathrm{GL}} + \nu(\nabla\mathbf{u}_N, \nabla\mathbf{v}_N)_{\mathrm{GL}} - (p_N, \nabla\cdot\mathbf{v}_N)_{\mathrm{G}} = (\mathbf{f}, \mathbf{v}_N)_{\mathrm{GL}} & \forall\mathbf{v}_{\mathrm{N}} \in X'_N \\ (q_N, \nabla\cdot\mathbf{u}_N)_{\mathrm{G}} = 0 & \forall q_N \in M'_N \end{cases} \tag{28}$$

where we choose the discrete velocity space X'_N and the discrete pressure space M'_N as follows:

$$X'_N = \{\mathbf{v} \in H_0^1(\Omega)^d;\ \mathbf{v}\big|_{\Omega^k} \in \mathbb{P}_N(\Omega^k)^d,\ k = -, +\}$$

$$M'_N = \{q \in L_0^2(\Omega);\ q\big|_{\Omega^k} \in \mathbb{P}_{N-2}(\Omega^k),\ k = -, +\}$$

As for the viscous/inviscid coupled problem (8), we arrive from (28) by expressing the discrete velocity and pressure in terms of Lagrangian interpolant bases through the Gauss–Lobatto and Gauss points respectively at the following matrix statements:

$$\mathbf{H}_v\mathbf{u}_v - \mathbf{D}_v^T p_v = \mathbf{B}_v\mathbf{f}_v \tag{29}$$

$$-\mathbf{D}_v\mathbf{u}_v = 0 \tag{30}$$

with

$$\mathbf{H}_v = \alpha\mathbf{B}_v + \nu\mathbf{A}_v$$

where $\mathbf{A}_v$ is the discrete Laplace opertor, $\mathbf{D}_v^T$ is the discrete gradient operator, $\mathbf{B}_v$ is the mass matrix corresponding to the global viscous problem.

Using the classical Uzawa algorithm, we obtain from the saddle problem (29) and (30) two positive definite symmetric similar to (24) and (25),

$$\mathbf{S}_v\mathbf{p}_v = -\mathbf{D}_v\mathbf{H}_v^{-1}\mathbf{B}_v\mathbf{f}_v \tag{31}$$

$$\mathbf{H}_v\mathbf{u}_v = \mathbf{D}_v^T\mathbf{p}_v + \mathbf{B}_v\mathbf{f}_v \tag{32}$$

where

$$\mathbf{S}_v = \mathbf{D}_v\mathbf{H}_v^{-1}\mathbf{D}_v^T \tag{33}$$

We solve the two systems (31) and (32) using the approach of Cahouet and Chabard, i.e. we solve Equations (31) and (32) by applying the nested inner/outer conjugate gradient algorithm with the pre-conditioner for the pressure matrix $\mathbf{S}_v$ [16],

$$\mathbf{P}_v = \alpha \mathbf{E}_v^{-1} + \nu \mathbf{B}_v^{-1} \tag{34}$$

where

$$\mathbf{E}_v = \mathbf{D}_v \mathbf{B}_v^{-1} \mathbf{D}_v^T \tag{35}$$

The particular choice (34) as a pre-conditioner for $\mathbf{S}_v$ can be motivated by considering two extreme situations of very small and very large values of α, i.e. the inverse of the time step. In both of these cases, $\mathbf{P}_v^{-1}\mathbf{S}_v$ is close to the identity matrix. The matrix $\mathbf{E}_v$ is in fact the discrete consistent Poisson operator of explicit schemes. Numerical simulations, performed by Maday *et al.* [16], have shown that inverting $\mathbf{E}_v$ requires more iterations than inverting a standard Laplace operator. There are, however, some recently developed approaches (see Fischer [25]) that make the $\mathbf{E}_v$ operator behave much like a standard Laplacian. To our aims, $\mathbf{E}_v$ is inverted using standard conjugate gradient iteration, although an overlapping Schwarz pre-condition is to be prepared.

The choice of $\mathbf{P}_v$ as a pre-conditioner for $\mathbf{S}_v$ leads to looking for a similar pre-conditioner for the viscous/inviscid coupled pressure matrix $\mathbf{S}_c$. If the interface operator $\mathbf{I}^\Gamma$ is absent from the systems (24) and (25), then the viscous part and the inviscid part would be completely separated. In this case we could pre-condition the two parts individually: $\alpha(\mathbf{D}^-(\mathbf{B}^-)^{-1}(\mathbf{D}^-)^T)^{-1} + \nu(\mathbf{B}^-)^{-1}$ for the viscous part, and $\alpha(\mathbf{D}^+(\mathbf{B}^+)^{-1}(\mathbf{D}^+)^T)^{-1}$ for the inviscid part. Now that the viscous and inviscid part are coupled through the interface operator $\mathbf{I}^\Gamma$, it is natural to choose the pre-conditioner for $\mathbf{S}_c$ as

$$\mathbf{P}_c = \alpha \mathbf{E}_c^{-1} + \nu(\mathbf{B}^-)^{-1} \tag{36}$$

where

$$\mathbf{E}_c = \mathbf{D}_c \mathbf{B}_c^{-1} \mathbf{D}_c^T \tag{37}$$

Although the solution of $\mathbf{E}_c$ appears to involve nested solves, this is not the case, as $\mathbf{B}_c$ is diagonal. In fact, according to the definition of $\mathbf{D}_c$, $\mathbf{E}_c$ is equivalent to the discrete pseudo-Laplace operator defined on a Gauss mesh in Ω^- and a Gauss–Lobatto mesh in Ω^+. Hence, similar to $\mathbf{E}_v$, $\mathbf{E}_c$ can also be inverted using conjugate gradient iteration. Some remarks on the inversion of $\mathbf{E}_c$ and total computational complexity analysis will be given in Section 7.

5. NUMERICAL RESULTS

We demonstrate the pre-conditioned conjugate gradient algorithm on the simple problem (1) with the rectangular domain $\Omega^- = (-2, 0) \times (-1, 1)$, $\Omega^+ = (0, 2) \times (-1, 1)$ and $f_1 = \alpha(1 - x_2^2) + \cos(x_1)\sin(x_2)$, $f_2 = \sin(x_1)\cos(x_2)$. With these data, the problem (1)–(2) possesses an analytical solution

$$\begin{cases} u_1(x_1, x_2, t) = 1 - x_2^2 \\ u_2(x_1, x_2, t) = 0 \\ p^-(x_1, x_2, t) = \sin(x_1)\sin(x_2) - 2\nu x_1 \\ p^+(x_1, x_2, t) = \sin(x_1)\sin(x_2) \end{cases}$$

The numerical tests are first used to prove the effectiveness of the pre-conditioner $\mathbf{P}_c$. Figure 2 plots the residual as a function of the iteration number for $\alpha = 100$, $\nu = 0.001$, $N = 14$ for the unpre-conditioned conjugate gradient (CG) and pre-conditioned conjugate gradient (PCG) procedures to the discrete viscous/inviscid coupled pressure system. Considerable acceleration results from the pre-conditioner $\mathbf{P}_c$. We compare the results with the those obtained by the pre-conditioner $\mathbf{P}_v$ to the pure viscous pressure system. Figure 3 presents the convergence history for the conjugate gradient procedures to the pure viscous pressure system for the same values of α, ν and N. The results obtained are very similar to the ones presented by Maday *et al.* [16]. Both $\mathbf{P}_c$ for $\mathbf{S}_c$ and $\mathbf{P}_v$ for $\mathbf{S}_v$ lead to significant convergence rates, though the convergence of the unpre-conditioned conjugate gradient procedure for the viscous/inviscid coupled problem is slower than the pure viscous problem. Note, however, the number of degrees of freedom used in the former is $2 \times (N+1)^2$ as compared with $(N+1)^2(N-1)^2$ in the latter, because a higher polynomial is used in the unviscid sub-domain when solving the viscous/inviscid coupling.

The next test is related to the investigation of dependence on the polynomial degrees of the $\mathbf{P}_c$-PCG algorithm. We plot in Figure 4 the convergence history as a function of the iteration number for the outer $\mathbf{P}_c$-PCG procedure for various choices of the polynomial degrees N. The similarity of the convergence rate between various values of N is indicative of the resolution-independent convergence of the $\mathbf{P}_c$-PCG algorithm.

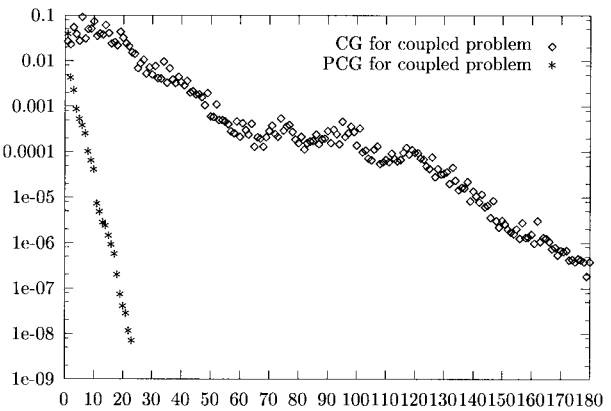

Figure 2. A plot of the residual as a function of the iteration number for the outer CG ($\diamond$) and P_c-PCG ($*$) procedures applied to spectral discretization pressure system of the viscous/inviscid coupled problem with $\alpha = 100$, $\nu = 0.01$, $N = 14$.

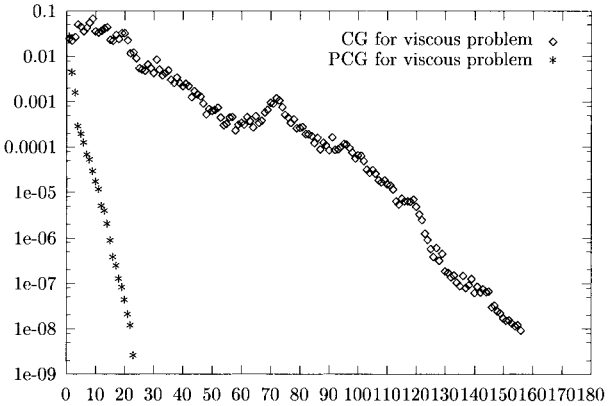

Figure 3. The convergence history for the outer CG ($\diamondsuit$) and P_v-PCG ($*$) procedures applied to spectral discretization pressure system of the pure viscous problem with $\alpha = 100$, $v = 0.01$, $N = 14$.

To demonstrate the effect of α on the properties of $\mathbf{P}_c\mathbf{S}_c$, we monitor the residual in the coupled pressure iteration for three different values of α. We plot in Figure 5 the convergence history for the outer $\mathbf{P}_c$-PCG procedure for various choices of values of α. As mentioned above, using $\mathbf{P}_c$ as the pre-conditioner for $\mathbf{S}_c$ is motivated by considering two extreme situations of very small and very large values of α. Hence, for the smaller and larger values of α, $\alpha = 1$ and $\alpha = 1000$, the discrete pressure operator $\mathbf{S}_c$ is perfectly pre-conditioned by $\mathbf{P}_c$, as shown in Figure 5. For the intermediate values of α, $\alpha = 100$, as expected in the pure viscous case, we see that the pre-conditioner $\mathbf{P}_c$ also does a good job, similar to the cases of $\alpha = 1$ and

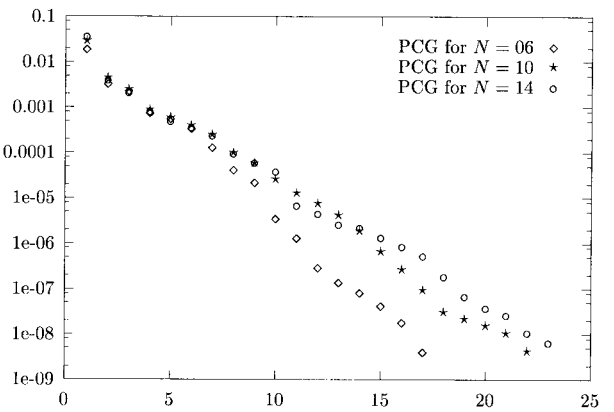

Figure 4. A plot of the residual as a function of the iteration number for the outer P_c-PCG procedures applied to the viscous/inviscid coupled problem for three different values of polynomial degree, $N = 6$ ($\diamondsuit$), $N = 10$ ($\bigstar$) and $N = 14$ ($\bigcirc$), with $\alpha = 100$, $v = 0.01$.

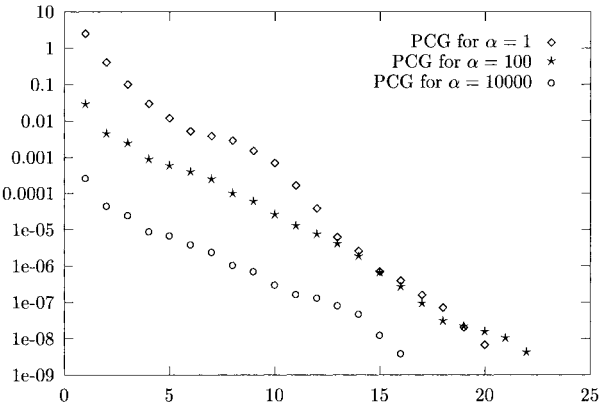

Figure 5. The convergence history as a function of the iteration number for the outer P_c-pre-conditioned conjugate procedures applied to the viscous/inviscid coupled problem for $\alpha = 1$ ($\diamondsuit$), $\alpha = 100$ ($\bigstar$) and $\alpha = 10000$ ($\bigcirc$), with $N = 10$ and $\nu = 0.01$.

$\alpha = 1000$. In conclusion, $\mathbf{P}_c$ is a good pre-conditioner for the discrete coupled pressure operator $\mathbf{S}_c$ for all values of α.

6. GENERALIZATION TO THE UNSTEADY NAVIER–STOKES/EULER COUPLED PROBLEM AND TO COMPLEX GEOMETRIES

As an essential building block, the viscous/inviscid coupled model presented above can be applied to the resolution of the unsteady Navier–Stokes/Euler coupled equations

$$\begin{cases} \dfrac{\partial \mathbf{u}^-}{\partial t} + (\mathbf{u}^- \cdot \nabla)\mathbf{u}^- - \nu \Delta \mathbf{u}^- + \nabla p^- = \mathbf{f}^-, \quad \nabla \cdot \mathbf{u}^- = 0 & \text{in } \Omega^- \times (0, T) \\ \dfrac{\partial \mathbf{u}^+}{\partial t} + (\mathbf{u}^+ \cdot \nabla)\mathbf{u}^+ + \nabla p^+ = \mathbf{f}^+, \quad \nabla \cdot \mathbf{u}^+ = 0 & \text{in } \Omega^+ \times (0, T) \end{cases} \tag{38}$$

where $(0, T)$ is the time interval ($T > 0$). In simulations of incompressible viscous fluid flow at moderate Reynolds numbers, the non-linear convective term is often treated explicitly, while the linear terms are treated implicitly (known as classic semi-implicit method). Numerous methods have been used in expressing of the convective operator when solving the pure Navier–Stokes equations by spectral element methods. Among them, the skew symmetric form and the rotational form have been preferred choices for transition and turbulence simulations, due to their good conservation properties. In particular, the rotational form conserves kinetic energy for inviscid flow, and requires evaluation of fewer derivatives. That was the motivation for using the rotational/semi-implicit method in our previous works [6,8] on the approximation

of the viscous/inviscid coupled problem. Some works by Horiuti [26], Zang [27] and Ronquist [28], however, indicate that the rotational form is less accurate than other forms. This point will be partially investigated in our numerical simulations. Moreover, the semi-implicit treatment of the convective terms has a principal restriction on the time step, in particular for convection-dominated flow. Recently, the operator–integration–factor splitting method has been becoming popular thanks to its better stability property as compared with the classic semi-implicit methods. This method, developed by Maday *et al.* [29], consists in decoupling the convective terms from the viscous and gradient operators in order to permit a much larger time step.

We adapt, in this section, the operator–integration–factor method to our viscous/inviscid coupled equations. Precisely, we first write Equation (38) into the following form:

$$\begin{cases} \dfrac{\mathrm{D}\mathbf{u}^-}{\mathrm{D}t} - \nu\Delta\mathbf{u}^- + \nabla p^- = \mathbf{f}^-, \quad \nabla\cdot\mathbf{u}^- = 0 & \text{in } \Omega^- \times (0, T) \\ \dfrac{\mathrm{D}u^+}{\mathrm{D}t} + \nabla p^+ = \mathbf{f}^+, \quad \nabla\cdot\mathbf{u}^+ = 0 & \text{in } \Omega^+ \times (0, T) \end{cases} \tag{39}$$

where $\mathrm{D}/\mathrm{D}t$ is the total derivative in the direction $\mathbf{u}$. We discretize (39) in time by an implicit scheme and so arrive at the following viscous/inviscid model:

$$\begin{cases} \alpha\mathbf{u}^{-n+1} - \nu\Delta\mathbf{u}^{-n+1} + \nabla p^{-n+1} = \mathbf{f}^{-n+1} + \alpha\mathbf{u}^{-n}(\chi^n(\cdot)), \quad \nabla\cdot\mathbf{u}^{-n+1} = 0 & \text{in } \Omega^- \\ \alpha\mathbf{u}^{+n+1} + \nabla p^{+n+1} = \mathbf{f}^{+n+1} + \alpha\mathbf{u}^{+n}(\chi^n(\cdot)), \quad \nabla\cdot\mathbf{u}^{-n+1} = 0 & \text{in } \Omega^+ \end{cases} \tag{40}$$

where $\alpha = 1/\Delta t$, and $\chi^n(x) = \chi(x, (n+1)\Delta t;\ n\Delta t)$ is the solution of

$$\frac{\mathrm{d}\chi}{\mathrm{d}\tau} = \mathbf{u}^n(\chi), \quad \chi(x, t;\ t) = x \tag{41}$$

Each time step requires a viscous/inviscid coupled resolution plus a transport of the previous solutions on the characteristics. Note that $\mathbf{u}^n(\chi^n(\cdot))$ is nothing other than $\tilde{\mathbf{u}}(\cdot, t^{n+1})$, the solution at $\tau = t^{n+1}$ of the following problem:

$$\begin{cases} \dfrac{\partial\tilde{\mathbf{u}}(x,\tau)}{\partial\tau} = -\mathbf{u}(x,\tau)\cdot\nabla\tilde{\mathbf{u}}(x,\tau), \quad t^n < \tau < t^{n+1} \\ \tilde{\mathbf{u}}(x, t^n) = \mathbf{u}(x, t^n) \end{cases}$$

We use a fourth-order Runge–Kutta scheme to determine the characteristic solution. The simple convective form is used to treat the above advection term.

We solve the coupled problem (38) by a spectral element method within a complicated geometry. As a test problem we take a laminar flow over a backward-facing step that is broken

into a viscous region and an inviscid region and involves a large number of degrees of freedom. To show the efficiency of the pre-conditioned Uzawa algorithm described above in the case of complex problem, we will investigate the behaviour of the $\mathbf{P}_c$-pre-conditioned conjugate gradient procedure for the coupled pressure system. Moreover, the comparisons on accuracy between the rotational/semi-implicit method and the operator–integration–factor characteristic method are also performed.

We consider the cases of Reynolds number $Re = \tilde{u}(H-h)/\nu = 73$ and 191, where $\tilde{u}$ is the average velocity at the entrance, H and h are respectively the height of the outlet and the entrance. $H-h$ is the height of the step. The expansion ratio of the step is $h{:}H = 2{:}3$. The profile of the inflow boundary condition is taken as parabolic (Poiseuille flow). The outlet boundary is taken far away from the step (22 step heights) to impose an undisturbed Dirichlet condition at the outflow. The partition of the viscous and inviscid sub-domains and the Gauss–Lobatto spectral element mesh used in the calculation is shown in Figure 6. The domain is broken into 37 macro-elements. Nineteen elements are for the viscous equations, 18 elements are for the inviscid equations. Fine resolution is placed near the step in order to resolve the thin boundary layers and eddy structures expected in the vicinity of the step. If using a polynomial degree $N = 8$, the total number of degrees of freedom on the pressure system is 2389.

We first monitor the residual in the outer pressure iteration as a function of the iteration number during the first time step at $Re = 191$. In Figure 7 we plot the convergence history when using a polynomial degree $N = 8$ and using $\mathbf{P}_c$ as a pre-conditioner for three different time steps $\Delta t = 0.1$, $\Delta t = 0.01$ and $\Delta t = 0.001$. Here again we see that the pre-conditioner $\mathbf{P}_c$ does a good job for all time steps even for complex problems. In Figure 8 we plot the convergence history when using a time step $\Delta t = 0.001$ for three different polynomial degrees $N = 6$, $N = 8$ and $N = 10$. Note the convergence rate decreases slightly as the polynomial degree N increases.

Now we make a comparison between the rotational/semi-implicit method and the characteristic method for each of the two Reynolds numbers. Figure 9(a) and (b) shows the pressure contour lines with the rotational/semi-implicit method (top) and the characteristic method (bottom) for $Re = 73$ and 191 respectively. In both cases, the characteristic method gives better results: the characteristic scheme yields smoother pressure fields than the rotational/semi-implicit scheme. At Reynolds number $Re = 73$, the difference between the two methods is not so large, the flow structure is accurately resolved by both methods. At Reynolds number $Re = 191$, however, the difference is more significant because the rotational form produces errors that are more damaging than those stemming from the characteristic method. Our numerical experiment, furthermore, supports the conclusion reported by, among others, Horiuti [30], Zang [27] and Ronquist [28].

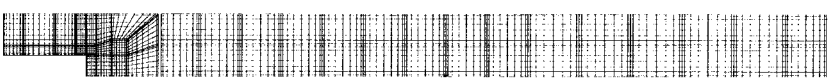

Figure 6. Partition of domain and spectral element mesh used for a laminar flow over a backward-facing step. The domain is broken into 37 macro-elements, of which 19 in the viscous part and 18 in the inviscid part.

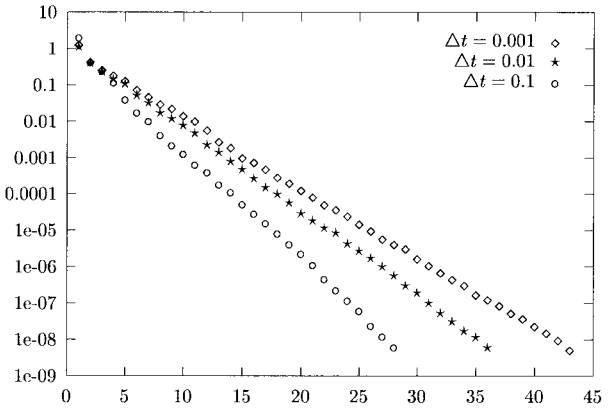

Figure 7. A plot of the residual as a function of the number of outer conjugate gradient iterations when solving for the first time step of a simulated laminar flow over a backward-facing step. The plot shows the convergence history when using polynomial degree $N = 8$ for three different time steps $\Delta t = 0.1$ (○), $\Delta t = 0.01$ (★) and $\Delta t = 0.001$ (◇).

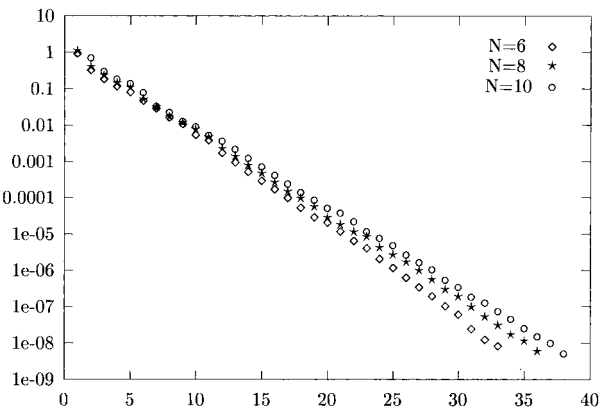

Figure 8. A plot of the residual as a function of the number of outer conjugate gradient iterations when solving for the first time step of a simulated laminar flow over a backward-facing step. The plot shows the convergence history when using time step $\Delta t = 0.01$ for three different polynomial degrees $N = 6$ (◇), $N = 8$ (★), and $N = 10$ (○). The convergence rate decreases slightly as the polynomial degree increases.

We compare also the result obtained by our coupled model with the ones obtained by the pure Navier–Stokes equations. We claim that choosing the backward-facing step laminar flow as our test problem, and partitioning the computational domain (as shown in Figure 6) is not indicative that we suppose the flow far downstream can be modelled by the inviscid Euler equation; rather, we hope that the calculation using the current decomposition may be used to

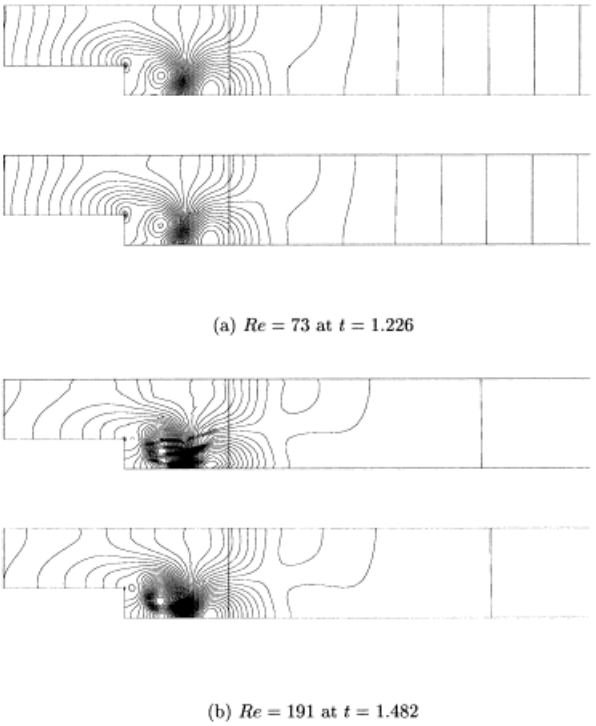

Figure 9. Pressure contour lines for laminar flow past a backward-facing step obtained by the rotational/semi-implicit method in both cases of Reynolds number.

analyse the viscous effect region and help us to determine where and when the viscous model can be reduced into the inviscid model. In fact, for laminar flow, at any Reynolds number, the flow may be entirely determined by the viscous–pressure balance. This fact will be confirmed by our following numerical results. Figures 10 and 11 show the velocity vectors distribution and streamline contours computed using the coupled model (top) and pure Navier–Stokes model (bottom) for two Reynolds numbers mentioned above respectively. Also shown are enlarged views of the streamline pattern near the step. Good agreement between the two models can be observed for both cases of $Re = 73$ and 191. This means that the viscous effect on the velocity field far downstream is small. Moreover, the agreement on eddy structures in the vicinity of the step observed via the enlarged view proves that the Navier–Stokes zone are well resolved using both our coupled model and the pure Navier–Stokes model.

To compare in detail the simulated flows computed by two models, we plot in Figure 12 the u_1 velocity profiles at various sections behind the step for $Re = 73$ and 191. The pressure profiles have also been plotted in Figure 13 for comparison. The u_1 velocity profiles resulting from the two models (solid lines for the coupled model, dotted lines for the pure viscous model) at each section coincide perfectly for both Reynolds number. For the pressure profiles,

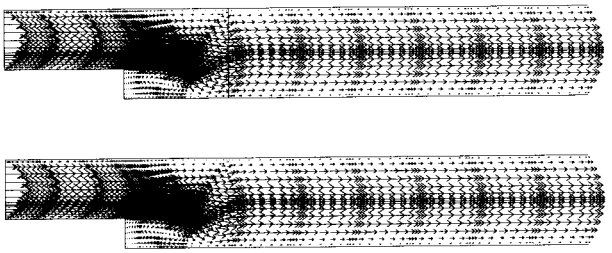

(a) $Re = 73$ at $t = 1.226$

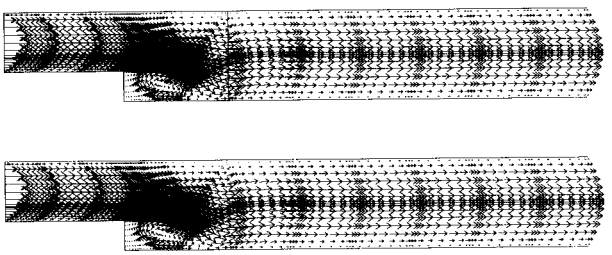

(b) $Re = 191$ at $t = 1.482$

Figure 10. Instantaneous velocity vector distribution obtained by the present coupled model (top of (a) and (b)) and pure viscous model (bottom of (a) and (b)). The results compare well for both Reynolds numbers $Re = 73$ and $Re = 191$.

there is also good agreement in the region between the step and the interface separating the viscous sub-domain and inviscid sub-domain (see Figure 6 for exact location of the interface). The significant differences observed on the pressure profiles are in the region behind the interface, where the pressure prediction of the coupled model is greater than that of the pure viscous model. The difference observed for Reynolds number $Re = 73$ is more significant than the one for Reynolds number $Re = 191$. The smaller the Reynolds number is, the greater the viscous term is. In this case, the viscous effect is no longer negligible as compared with the values of the pressure behind the interface (note that the pressure near the outlet is small, of order $O(10^{-3})$ in our examples). Careful examinations show that the full viscous pressure prediction is a linear decrease, whereas the viscous/inviscid coupled pressure prediction is a constant in the inviscid sub-domain. This may be due to the fact that, in a laminar flow, existence of the boundary layer makes the viscous diffusion no longer negligible even if the viscosity is small. Even so, we believe that if we are only interested in the fluid movement in the vicinity of the step (this is often the case in practice), the current location of the interface has been able to give sufficiently good results near the step, at least comparable with the those obtained from the full Navier–Stokes equations within the whole domain.

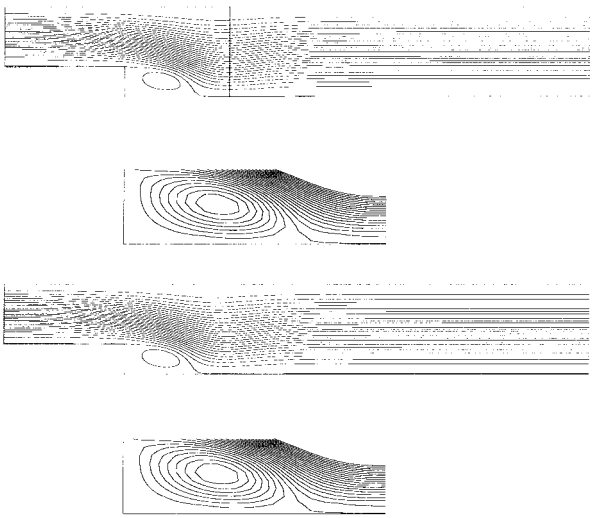

(a) $Re = 73$ at $t = 1.226$

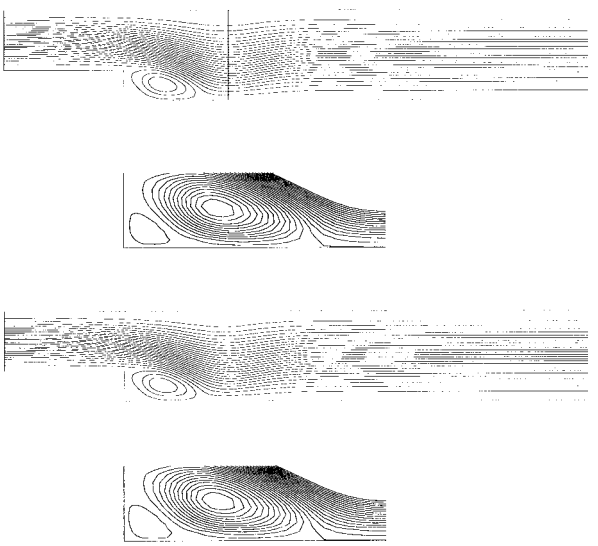

(b) $Re = 191$ at $t = 1.482$

Figure 11. Streamline contours obtained by the present coupled model (top of (a) and (b)) and pure viscous model (bottom of (a) and (b)). Eddy structures in the vicinity of the step are enlarged for better comparisons. The results are comparable between the two.

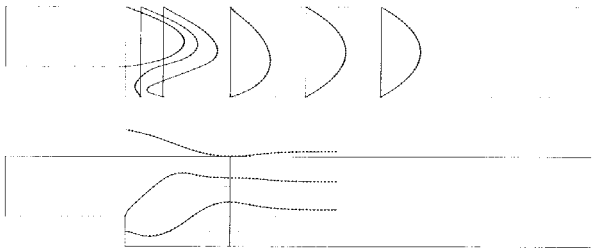

(a) $Re = 73$ at $t = 1.226$

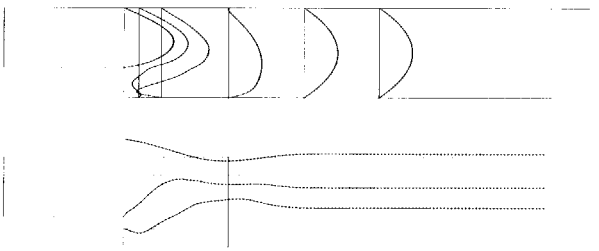

(b) $Re = 191$ at $t = 1.482$

Figure 12. Horizontal velocity profiles plotted at various sections behind the step computed respectively by the present coupled model (solid lines) and pure viscous model (dotted lines).

The profiles at the horizontal sections (bottom parts in Figures 12 and 13) are used to show the behaviours of the flow neat the interface. It can be noticed from the two bottom figures that the flow traverses continuously the interface. This is indicative that the interface conditions are well resolved by the mesh we used.

We now make some remarks regarding the partition of the viscous and inviscid sub-domains. For our purposes, the partition is made artificially for a reason that the main purposes of our numerical experiments are to show the effectiveness and potential of the proposed method. In real applications, the exact location of the interface would be non-trivial. There are still a number of open mathematical questions related to the behaviour of the solutions when the Reynolds number increases. The convergence of the solution of the Navier–Stokes equations to the solution of the Euler equations when the Reynolds number tends to infinity has been proved only in very special cases (the external flow is one of these cases, in which the Euler equations are really appropriate in a region far from the obstacle). The main difficulty is to understand how the boundary conditions behave in the limiting process. According to the viewpoint of Brezzi *et al.* [30], neglecting the diffusion effects in the Navier–Stokes equations is justified only in the region where the divergence of the stress

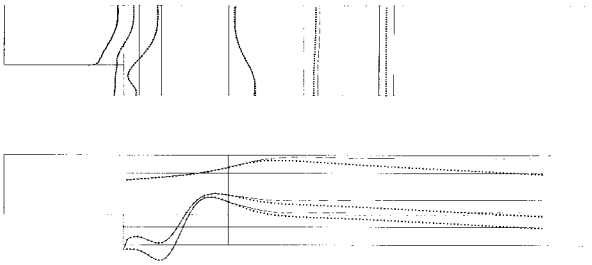

(a) $Re = 73$ at $t = 1.226$

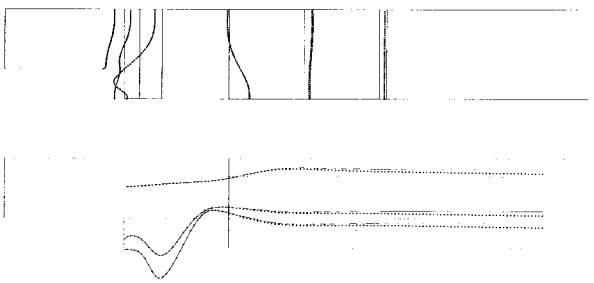

(b) $Re = 191$ at $t = 1.482$

Figure 13. A plot of the pressure profiles at various sections behind the step computed respectively by the present coupled model (solid lines) and pure viscous model (dotted lines).

tensor is negligible, i.e. if, for a constant Reynolds number, $(1/Re)\Delta\mathbf{u}$ is negligible. This means that even for moderate Reynolds number, it is also possible to reduce the Navier–Stokes equations to the Euler equations in the region if $(1/Re)\Delta\mathbf{u}$ is smaller than an optimistic estimate of the discretization error. In this sense, it is expected that the present viscous/inviscid coupled model can be used as a tool to the viscous/inviscid analysis.

7. COMPUTATIONAL COMPLEXITY COMPARISON

Now we are in a position to compare the computational complexity of solving the viscous/inviscid coupled system (24)–(25) and the global viscous system (31)–(32). We first summarize the main computational procedure. We are in fact solving the following systems:

$$\mathbf{Sp} = -\mathbf{DH}^{-1}\mathbf{Bf} \tag{42}$$

$$\mathbf{Hu} = \mathbf{D}^T\mathbf{p} = \mathbf{Bf} \tag{43}$$

which can be the system (24)–(25) or the system (31)–(32). The outer pre-conditioned conjugate gradient iteration for the pressure system (42) takes the following form (see e.g. [18]):

$$\mathbf{p}_0, \qquad \mathbf{r}_0 = \mathbf{S}\mathbf{p}_0 - \mathbf{D}\mathbf{H}^{-1}\mathbf{B}\mathbf{f}, \qquad \mathbf{g}_0 = \mathbf{P}\mathbf{r}_0, \qquad \mathbf{d}_0 = \mathbf{g}_0$$

$$a_m = -\frac{\mathbf{g}_m^T\mathbf{r}_m}{\mathbf{d}_m^T\mathbf{S}\mathbf{d}_m}$$

$$\mathbf{p}_{m+1} = \mathbf{p}_m + a_m\mathbf{d}_m, \qquad \mathbf{r}_{m+1} = \mathbf{r}_m + a_m\mathbf{S}\mathbf{d}_m$$

$$\mathbf{g}_{m+1} = \mathbf{P}\mathbf{r}_{m+1}, \qquad b_m = \frac{\mathbf{g}_{m+1}^T\mathbf{r}_{m+1}}{\mathbf{g}_m^T\mathbf{r}_m}$$

$$\mathbf{d}_{m+1} = \mathbf{r}_{m+1} + b_m\mathrm{d}_m$$

where $\mathbf{P}$ is the pre-conditioner, m is the iteration counter, $\mathbf{r}_m$ is the residual, $\mathbf{g}_m$ is a vector associated with the pre-conditioning, $\mathbf{d}_m$ is the search direction, and a_m and b_m are scalars. The inner pre-conditioned conjugate gradient iteration is related to the evaluation of the matrix–vector product $\mathbf{Sd}$ in the outer conjugate gradient iteration. This evaluation is achieved as follows:

$$\mathbf{y} = \mathbf{D}^T\mathbf{d}$$
$$\mathbf{Hz} = \mathbf{y}$$
$$\mathbf{Sd} = \mathbf{Dz}$$

Each matrix–vector product evaluation requires d standard Helmholtz solvers in the d-dimensional case. The evaluation of the preconditioning $\mathbf{Pr}$ needs one inversion of the matrix $\mathbf{E}$ and one inversion of the mass matrix $\mathbf{B}$. Note that the mass matrix $\mathbf{B}$ is diagonal, the cost of the pre-conditioning in each iteration of the outer iteration lies on the inversion of $\mathbf{E}$. Therefore, each iteration in the outer conjugate gradient iteration requires one pseudo-Laplacian solver for $\mathbf{E}_c$ in whole domain Ω and d standard Helmholtz solvers in the viscous sub-domain Ω^- for the viscous/inviscid coupled case, as compared with one pseudo-Laplacian solver for $\mathbf{E}_v$ and d standard Helmholtz solvers all in whole domain Ω for the pure viscous case.

If the condition numbers of the matrix $\mathbf{P}_c\mathbf{S}_c$ and $\mathbf{P}_v\mathbf{S}_v$ are respectively of order say $O(r_c)$ and $O(r_v)$, then the number of outer conjugate gradient iterations scales like $O\sqrt{r_c}$ for $\mathbf{P}_c\mathbf{S}_c$ and $O(\sqrt{r_v})$ for $\mathbf{P}_v\mathbf{S}_v$. We see hence that computing the pressure requires only order $\sqrt{r_v}$, pseudo-Laplacian solver in the whole domain Ω and $\sqrt{r_c}d$ standard Helmholtz solvers in the viscous sub-domain Ω^- for the viscous/inviscid coupled case, as compared with order $\sqrt{r_v}d$ pseudo-Laplacian solver and $\sqrt{r_v}d$ standard Helmholtz solvers, all in the whole domain Ω for the pure viscous case. Once the pressure is known, another d standard Helmholtz solvers in the *viscous* sub-domain Ω^- is needed to compute the velocity for the viscous/inviscid coupled case,

as compared with d standard Helmholtz solvers in the whole domain Ω^- needed for the pure viscous case.

It is well known that [24,31], by using a tensor product factorization technique, one Laplacian operator in d space dimensions can be evaluated by $O(N^{d+1})$ operations for each macro-element. If the inner pre-conditioned conjugate gradient algorithm is employed to solve the discretized Helmholtz equations, and suppose that the number of iterations required to achieve convergence scales is τ_H, then the approximate operation count for a solution of a standard Helmholtz problem in $\mathbb{R}^d$ is $O(\tau_H N^{d+1})$ in each macro-element. The final approximate operation count for a solution of Equations (24) and (25) by outer–inner pre-conditioned conjugate gradient algorithm is thus of the order

$$\sqrt{\tau_c}\tau_E K N^{d+1} + \sqrt{r_c} d\tau_H K^- N^{d+1}$$

that is

$$\sqrt{r_c} N^{d+1}(\tau_E K + d\tau_H K^-)$$

for the viscous/inviscid coupled case, as compared with order

$$\sqrt{r_v}\tau_E K N^{d+1} + \sqrt{\tau_v} d\tau_H K N^{d+1} = \sqrt{\tau_v} K N^{d+1}(\tau_E + d\tau_H)$$

for the pure viscous case, where it is supposed that the inversions of E_c and E_v require the same number of iterations, say τ_E. K and K^- are respectively the total macro-element number and macro-element number in the viscous region. The cost rate τ between the coupled model and the pure viscous model is then

$$\tau = \frac{\sqrt{\tau_c} N^{d+1}(\tau_E K + d\tau_H K^-)}{\sqrt{r_v} K N^{d+1}(\tau_E + d\tau H)} = \sqrt{\frac{\tau_c}{r_v}}\left(\frac{\tau_E}{\tau_E + d\tau_H} + \frac{K^-}{K}\frac{d\tau_H}{\tau_E + d\tau_H}\right)$$

In real applications, K^- could be small as compared with K, so the cost rate scales like $\sqrt{\tau_c/\tau_v}\tau_E/(\tau_E + d\tau_H)$. It is expected, and confirmed by our numerical test (see Figures 2 and 3), that τ_c and τ_v have the same order. As a result, the cost rate behaves like $\tau_E/(\tau_E + d\tau_H)$.

Finally, we make some remarks regarding the inversion of the pseudo-Laplacian matrix $\mathbf{E}$. From the definitions of $\mathbf{E}_c$ and $\mathbf{E}_v$ in Equations (37) and (35) respectively, we see that the matrices $\mathbf{E}_c$ and $\mathbf{E}_v$ are practically of same structure. They are essentially a second-order operator with Neumann-like pressure boundary conditions. In our calculation, standard conjugate gradient iteration has been used to invert both $\mathbf{E}_c$ and $\mathbf{E}_v$. The experience from numerical simulations has been that inverting $\mathbf{E}_c$ and $\mathbf{E}_v$ needs more iterations than inverting the standard Laplace operator or Helmholtz operator (but the difference between $\mathbf{E}_c$ and $\mathbf{E}_v$ has been very slight), i.e. $\tau_E > \tau_H$. There are, however, some recent overlapping Schwarz pre-conditioners for the $\mathbf{E}$ system, developed by Fischer [25], which make the inversion of the $\mathbf{E}$ matrix behave much more like a standard Laplace matrix. We plan to employ his approach in our future implementation in order to make our method more competitive.

8. DISCUSSIONS AND CONCLUSIONS

In conclusion, an efficient pre-conditioned Uzawa algorithm has been analysed and applied to spectral element approximation of the Navier–Stokes/Euler coupled equations. The numerical examples demonstrate the applications of the present algorithm to the simulations of incompressible flow problems. It is shown, from our numerical simulations, that the present algorithm has been able to reduce the computational cost. The computational complexity analysis shows that, using the global pseudo-Laplace operator as a pre-conditioner, the cost rate between the coupled model and the pure viscous model depends on the efficient inversion of the pseudo-Laplacian. More the inversion of the pseudo-Laplacian behaves like the inversion of a standard Laplacian or a standard Helmholtz operator, further reduction on the computational cost is gained using the present viscous/inviscid coupled model. Further work will be related to find a more effective approach to invert the pseudo-Laplacian operator. We note also that if we want to reduce the computational cost further, we would have to use another pre-conditioner other than the global pseudo-Laplace operator. Better pre-conditioners will be the ones that use only the local information in the viscous region. We are also planning to address these problems in a future paper.

ACKNOWLEDGMENTS

This work was supported by the Natural Science Foundation of China, under grant K16017.

REFERENCES

1. Canuto C, Hussaini MY, Quarteroni A, Zang ZA. *Spectral Methods in Fluid Dynamics*. Springer: New York, 1987.
2. Bourgat JF, Le Tallec P, Mallinger F, Perthame B, Qiu Y. *Couplage Boltzmann Navier–Stokes*. Preprint, INRIA, 1994; 2281.
3. Gastaldi F, Quarteroni A, Sacchi Landriani G. Effective methods for the treatment of interfaces separating equations of different character. In *Computers and Experiments in Fluid Flow*, Carlomagno GM, Brebbia CA (eds). Springer: Berlin, 1989; 65.
4. Quarteroni A, Valli A. *Numerical Approximation of Partial Equations*. Springer Series in Computational Mathematics, vol. 23. Springer: Berlin, 1994.
5. Dinh QV, Glowinski R, Periaux J, Terrasson G. On the coupling of viscous and inviscid models for incompressible fluids via domain decomposition. In *Proceedings of the 1st Symposium on Domain Decomposition*, Paris, 1987.
6. Xu CJ. *Couplage des équations de Navier–Stoke et d'Euler*. PhD Thesis, Université de Pierre et Marie Curie, 1993.
7. Xu CJ. A global algorithm on the coupling of viscous/inviscid equations. In *Proceedings of 3rd International Conference on Spectral and High Order Methods*, *Houston*, *1995. Houston Journal of Mathematics* 1996; 151.
8. Xu CJ, Maday Y. Coupling of the Navier–Stokes and Euler equations: resolution by a spectral method. In *Conference on Scientific and Engineering Computing*. National Defence Industry Press: Beijing, 1994.
9. Morchoisne Y. Inhomogeneous flow calculations by spectral methods: mono-domain and multidomain techniques. In *Spectral Methods for Partial Differential Equations*, Voigt RG, Gottlieb D, Hussaini MY (eds). SIAM-CBMS; 181.
10. Yamaguchi Y, Cheng CJ, Brown RA. Multiple buoyancy-driven flows in a vertical cylinder heated from below. *Philosophical Transactions of the Royal Society*, *London* 1984; **A312**: 519.
11. Wathen A, Silvester D. Fast iterative solution of stabilised Stokes systems. *SIAM Journal of Numerical Analysis* 1993; **30**(3): 630.
12. Glowinski R, Pironneau O. On a mixed finite element approximation of the Stokes problem. *Numerical Mathematics* 1979; **33**: 397.

13. Kim J, Moin P. Application of a fractional-step method to incompressible Navier–Stokes equations. *Journal of Computational Physics* 1985; **59**: 308.
14. Kleiser L, Schumann U. Spectral simulation of the laminar turbulent transition process in plane Poiseuille flow. In *Spectral Methods for Partial Differential Equation*, Voigt RG, Gottlieb D, Hussaini MY (eds). SIAM, 1984.
15. Orszag SA, Israeli M, Deville MO. Boundary condition for incompressible flows. *Journal of Scientific Computing* 1986; **1**: 75.
16. Maday Y, Meiron D, Patera AT, Ronquist EM. Analysis of iterative methods for the steady and unsteady Stokes problem: application to spectral element discretization. *SIAM Journal of Science and Computers* 1993; **14**(2): 310.
17. Brezzi F. On the existence, uniqueness and approximation of saddle-point problem arising from Lagrange multipliers. *RAIRO Analyse Numérique* 1974; **8**(R2): 129.
18. Girault V, Raviart PA. *Finite Element Approximation of the Navier–Stokes Equations*. Springer: New York, 1987.
19. Xu CJ. An iterative method for the Navier–Stokes/Euler coupled equations. *Journal of Computational Mathematics* 1999; **17**(4): 379.
20. Bernardi C, Maday Y. *Approximations Spectrales de Problèmes aux Limites Elliptiques*. Springer: Paris, 1992.
21. Debit N, Maday Y. The coupling of spectral and finite element methods for the approximation of the Stokes problem. In *Proceedings of the 8th France–USSR–Italy Joint Symposium*, Pavie, Italy, 1989.
22. Cahouet J, Chabard JP. Some fast 3D finite elements solvers for the generalized Stokes problem. *International Journal for Numerical Methods in Fluids* 1988; **8**: 869.
23. Fischer P, Ronquist E, Dewey D, Patera AT. Spectral element methods: algorithms and architectures. In *1st International Symposium on Domain Decomposition Methods for Partial Differential Equations*, SIAM, 1987; 173.
24. Maday Y, Patera AT. Spectral element methods for the Navier–Stokes equations. In State-of-the-art Surveys in Computational Mechanics, Noor AK (ed). ASME: New York, 1988; 71.
25. Fischer P. An overlapping Schwarz method for spectral element solution of the incompressible Navier–Stokes equations. *Journal of Computational Physics* 1997; **133**: 84.
26. Horiuti K. Comparison of conservative and rotational forms in large eddy simulation of turbulent channel flow. *Journal of Computational Physics* 1987; **71**: 343.
27. Zang AT. On the rotational and skew-symmetric forms for incompressible flow simulations. *Applied Numerical Mathematics* 1991; **7**: 27.
28. Ronquist EM. *Optimal spectral element methods for the unsteady three-dimensional incompressible Navier–Stokes equations*. PhD Thesis, Massachusetts Institute of Technology, 1988.
29. Maday Y, Patera AT, Ronquist EM. An operator–integration–factor splitting method for time-dependent problems: application to incompressible fluid flow. *Journal of Scientific Computing* 1990; **5**(4): 263–292.
30. Brezzi F, Canuto C, Russo A. A self-adaptive formulation for the Euler/Navier–Stokes coupling. *Computational Methods in Applied Mechanics and Engineering* 1989; **73**: 317.
31. Orszag SA. Spectral methods for problems in complex geometries. *Journal of Computers and Physics* 1980; **37**: 75.
32. Marini LD, Quarteroni A. A relaxation procedure for domain decomposition methods using finite elements. *Numerical Mathematics* 1989; **55**: 575.

